14th Australasian Fluid Mechanics Conference
Adelaide University, Adelaide, Australia
10-14 December 2001

Symmetry Breaking to Modulated Rotating Waves in an Enclosed Swirling Flow

H. M. Blackburn[1] **and J. M. Lopez**[2]

[1]CSIRO Building Construction and Engineering
PO Box 56, Highett, Victoria, 3190 AUSTRALIA

[2]Department of Mathematics
Arizona State University, Tempe, AZ, 85287 USA

Abstract

Rotating waves are a generic instability mode of flows that possess a rotation symmetry, such as Taylor–Couette flow. In the enclosed swirling flow that is generated in a closed cylindrical container by a rotating endwall, the initial bifurcation to unsteadiness produced by increasing the endwall rotation rate can be either to rotating waves or unsteady axisymmetric flow, depending on the aspect ratio of the cylinder. We examine a case where the initial bifurcation is to a periodic axisymmetric state, and follow subsequent bifurcations to other states where the flow breaks axisymmetry as well. These resulting states possess rotating waves that are modulated by the underlying axisymmetric behaviour. Although this flow also has axial vortex breakdowns, they appear to play no dynamical role in the symmetry breaking, remaining essentially axisymmetric.

Introduction

Flows of Newtonian fluid generated inside a closed cylindrical container by the steady rotation of one endwall are interesting as prototypical swirling flows, the cylindrical coordinate equivalent of the rectangular driven cavity. There are two control parameters: the cylinder aspect ratio $\Lambda = H/R$, where H is the height and R the radius of the cylinder, and the Reynolds number $Re = \Omega R^2/\nu$, where Ω is the endwall rotation rate and ν the kinematic viscosity.

Following the work of Vogel [9] which identified a vortex breakdown (a region of reversed axial flow) on the cylinder axis in such flows, Escudier [3] established the envelope of cylinder aspect ratios and Reynolds numbers within which axial vortex breakdowns are observed. At any value of Λ, the flows exhibit no breakdowns as $Re \to 0$; for $\Lambda \gtrsim 1$, one or more breakdowns may be observed as Re is increased. The flows with breakdowns are steady and axisymmetric at Reynolds numbers below the onset of instability. With further increase in Reynolds number the flow becomes unsteady via Hopf bifurcation in one of two alternative ways, either by production of symmetry-breaking rotating waves (RWs), where the flow is steady when viewed in an appropriate rotating frame of reference, or by unsteady periodic behaviour where axisymmetry is preserved. The choice between these two alternatives is determined by the cylinder aspect ratio Λ.

General three-dimensional perturbations to the axisymmetric, steady basic state have been examined in the linear stability analysis of Gelfgat *et al.* [4] for the range $1 < \Lambda < 4$. For low aspect ratios, $1 < \Lambda < 1.63$, the analysis predicts symmetry breaking via a Hopf bifurcation to a RW state with azimuthal wavenumber $k = 2$. For high aspect ratios, $\Lambda > 2.76$, the analysis again predicts a symmetry-breaking Hopf to a RW with $k = 4$. At intermediate aspect ratios, the predicted initial bifurcated state retains axisymmetry, but is time-periodic. Near the boundaries $\Lambda = 1.6$, 2.8, double-Hopf bifurcations can occur, as shown in [7] for $\Lambda \simeq 1.6$. Here we use direct numerical simulation to investigate the flow for a fixed aspect ratio $\Lambda = 2.5$ at which the first bifurcation to occur with increasing Re is a supercritical Hopf that preserves the axisymmetry.

Computational Methods

The numerical method adopted for this study employs spectral elements for the discretisation of the meridional semi-plane, coupled with Fourier expansions in azimuth, and a mixed implicit–explicit second order time integration scheme. The use of Fourier expansions in the azimuthal direction preserves the $SO(2)$ rotation symmetry of the continuous system within the discretised one. The mesh employs 60 spectral elements, concentrating resolution in the boundary layers and in particular at the boundary condition discontinuity where the spinning end-wall meets the stationary cylindrical wall. The interpolation order within each element was established on the basis of a convergence study conducted at $Re = 4000$; each element employs a two-dimensional tensor product of 7th-order Gauss–Lobatto–Legendre Lagrange shape functions. The number of Fourier modes employed in azimuth was varied between five and 64; the presented results employ the equivalent of 20 or more modes. For further details of the numerical method, consult [2].

Evolution of the computed solutions is monitored through a variety of runtime diagnostics. Central to the current investigation is the (dimensionless) amount of flow kinetic energy contained in each Fourier mode k

$$E_k = \frac{1}{2A\Omega^2R^2}\int_A \hat{\boldsymbol{u}}_k \cdot \hat{\boldsymbol{u}}_k^* \, r \, \mathrm{d}A, \qquad (1)$$

where A is the area of the two-dimensional meridional semi-plane and $\hat{\boldsymbol{u}}_k^*$ denotes the complex conjugate of the velocity data in the kth Fourier mode. Energy of the axisymmetric part of the flow is represented by E_0.

To initiate three-dimensional solutions, a small amount of white noise (standard deviation approx. $10^{-12}R\Omega$) is added to the first non-zero Fourier mode and the solution evolved to statistical stationarity.

Results

As noted above, the first bifurcation to occur in this flow (for $\Lambda = 2.5$) as Reynolds numbers are increased is a supercritical Hopf that preserves axisymmetry; this occurs at $Re = 2707$ [4, 6]. Thereafter, while further solution branches appear, it is the underlying axisymmetric flow that dominates the behaviour in each case, up to the maximum Reynolds number for this study, $Re = 4300$.

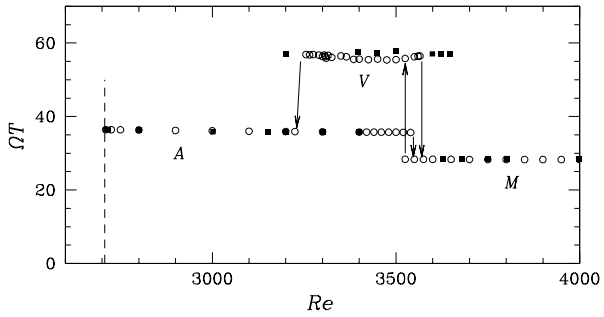

Figure 1: Fundamental oscillation periods for axisymmetric simulations (○), as a function of Reynolds number, with transitions between different solution branches indicated. Solutions on the V branch are quasiperiodic, with very-low-frequency modulations, while the A and M branches have periodic solutions. The dashed line at $Re = 2707$ indicates the Reynolds number for onset of unsteadiness at $\Lambda = 2.5$. Also shown (■) are the experimentally measured values [8].

Thus we first present results from simulations that are restricted to an axisymmetric subspace (a single Fourier mode, $k = 0$). These are shown in terms of the fundamental oscillation periods ΩT in figure 1, where three distinct solution branches may be observed. Also shown are experimentally measured values [8]; it can be seen that the axisymmetric values are very similar to the experimental ones, but that branch extents are slightly different. The three solution branches are labelled as: A (axisymmetric), for which our investigations show solutions are stable to three-dimensional perturbations; M, where the flow is periodic but unstable to three-dimensional perturbations, leading to RWs that are modulated by the axisymmetric behaviour (MRWs); and V, where the axisymmetric state has very-low-frequency (VLF) modulations in addition to the $\Omega T \simeq 57$ behaviour shown in figure 1. For some of its extent, we have found that the V branch is unstable to three-dimensional perturbations, again leading to MRWs. Experiments [8] show similar behaviour for each of these three branches, including the VLF modulation on the V branch.

Symmetry Breaking

It was established in [1] that at $Re = 3500$ and $Re = 4000$, the axisymmetric flows were unstable to three-dimensional perturbations, leading to MRWs on the V and M solution branches respectively, with minimal modification to the dominant fundamental periods shown in figure 1. In both cases the MRW structure was strongly periodic in azimuth, with a 5-fold azimuthal symmetry for the V branch solution and a 6-fold symmetry for the M branch. These symmetry indices are used to further classify the solutions obtained as V_5 and M_6. The MRW structures are visualised in figure 2, which shows isosurfaces and extracted contours of azimuthal velocity for the two cases. The RW structures precess slowly around the container in the same sense as the rotating endwall.

The energy in the MRWs is strongly coupled to that in the axisymmetric component of the flow, as illustrated in figure 3, which displays energies in the axisymmetric component of the flow for example solutions on the A, V_5 and M_6 solution branches, and in the leading non-axisymmetric mode for the V_5 and M_6 solution branches. The VLF modulation present in solutions of the V branch

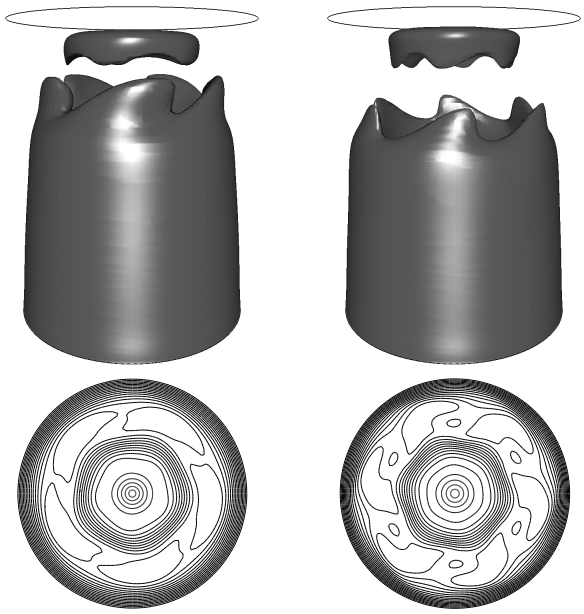

Figure 2: Rotating modulated waves of the (a) V_5, $Re = 3500$ and (b) M_6, $Re = 4000$ solutions, as manifest in the azimuthal velocity component. Above, perspective views of instantaneous isosurfaces—solid lines indicate extent of cylinder, and the bottom wall rotates clockwise when viewed from above; below, instantaneous contours at elevation $z/H = 0.8$.

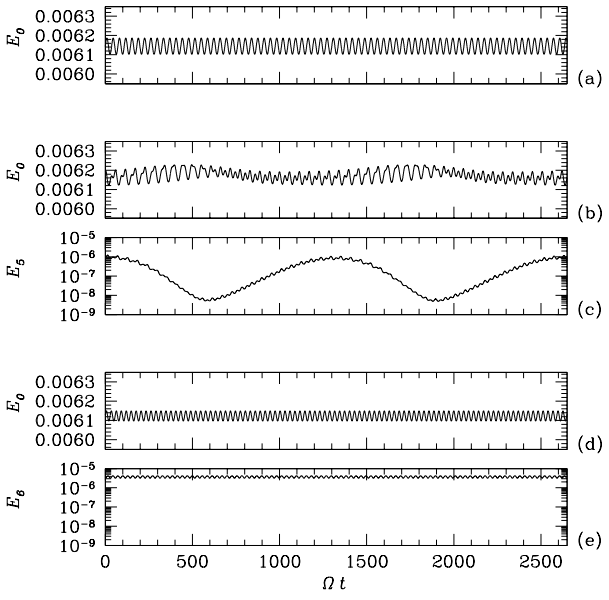

Figure 3: Time series of modal kinetic energies for the axisymmetric mode (E_0) and, if appropriate, for the leading nonaxisymmetric mode at (a) $Re = 3000$, A branch; (b, c) $Re = 3500$, V_5 branch; (d, e) $Re = 4000$, M_6 branch.

can be clearly seen; while this does not substantially alter the energy E_0, it produces a two-magnitude variation in E_5, superimposed over fluctuations with periods $\Omega T \simeq 57$ and 28.

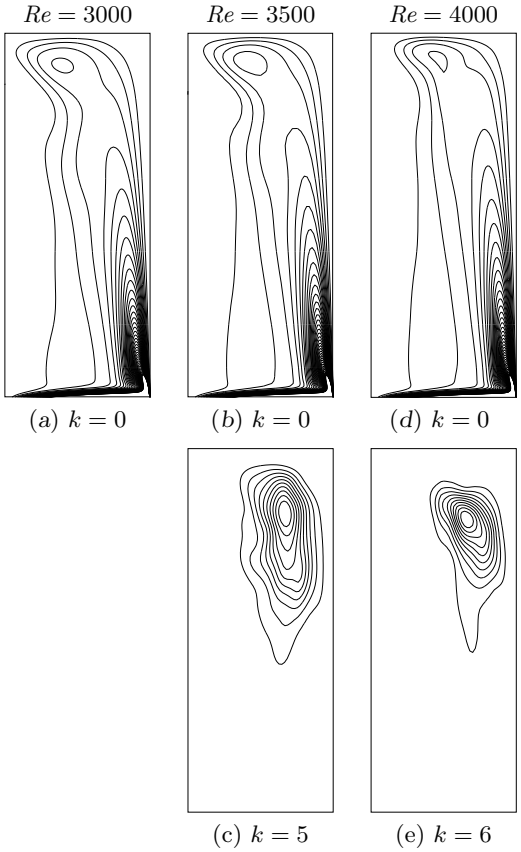

Figure 4: Contours of averaged flow kinetic energy $\langle \hat{\boldsymbol{u}}_k \cdot \hat{\boldsymbol{u}}_k^* \rangle / 2R^2\Omega^2$ in the meridional semi-plane for (a), $Re = 3000$; (b, c), $Re = 3500$; (d, e), $Re = 4000$. Upper, axisymmetric component; lower, energy in the leading non-axisymmetric mode. In each plot the cylinder axis is to the left and the rotating endwall is at the bottom.

The spatial localisation of the MRW energies is illustrated in figure 4, where contours of ensemble-average contributions to E_5 for the V_5 solution to E_6 for the M_5 solution are shown, and compared to contours of ensemble-average contributions to E_0. The MRW energies are concentrated near $r/R = 0.67$, $z/H = 0.8$, i.e. near the end of a cylindrical wall-jet that results from the deflection of the Ekman layer formed on the spinning endwall situated at $z = 0$. The peak energies are remote from the axis, where the flow remains essentially axisymmetric, as is also demonstrated by the contour plots of figure 2.

The M Branch

The M solution branch supports MRWs for all Reynolds numbers at which we were able to follow it, but it is unclear if it is unstable to non-axisymmetric perturbations at lower Reynolds number. At the lower Re-limit, both the axisymmetric and non-axisymmetric solutions on the M branch jump to solutions on the V branch.

In addition to the 6-fold symmetry apparent in figure 4, the M solution branch also supports MRWs with a 5-fold symmetry; initial conditions determine state selection. The energy levels of the leading non-axisymmetric modes are significantly lower for the M_6 states than for the M_5 states, as illustrated in figure 5, where the observed lower Re-limits of branch extents for these non-axisymmetric solutions are also shown (cf. figure 1).

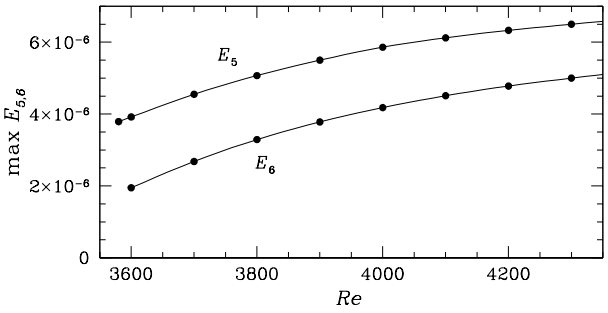

Figure 5: Peak energies of leading non-axisymmetric mode on the M_5 and M_6 branches.

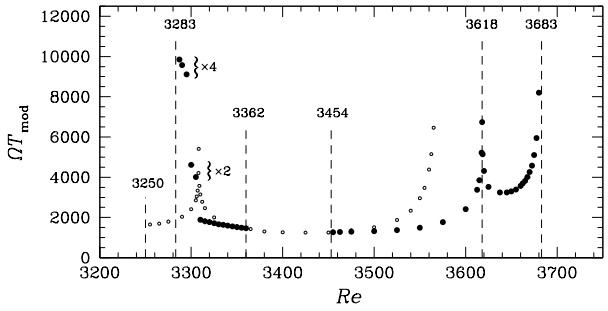

Figure 6: VLF modulation periods on the V branch. •, V_5; ◦, V_0. Note period-doubled and quadrupled values near $Re = 3300$.

The V Branch

Solutions of the V branch possess richer dynamics than the M branch. Figure 6 shows the VLF modulation periods observed on this branch, both for the axisymmetric restriction (hollow symbols) and the states which break axisymmetry (solid symbols). We have observed only 5-fold-symmetric wave states on this solution branch. It can be seen that there are two disjoint Re-ranges for symmetry-breaking on the V branch: 3283–3362 and 3454–3683. At the central limits $Re = 3362$ and 3454, the V_5 solutions asymptote to the V_0 axisymmetric state. On the upper V_5 branch, $\Omega T_{\rm mod} \to \infty$ at a single cusp located at $Re = 3618$, but the branch continues until $Re = 3683$, where again $\Omega T_{\rm mod} \to \infty$. Here the solutions become M_5 states, as the $\Omega T \simeq 57$ frequency loses dominance to $\Omega T \simeq 28$, which was also present in the spectrum. On the lower V_5 branch, the VLF modulation period-doubles, then doubles again before we lose the branch at $Re = 3283$ and the axisymmetry of the V_0 state is regained.

Figure 7 shows the Re-variation of peak energy in the $k = 5$ mode on the V_5 branch. This plot emphasises the return to axisymmetry (V_0) for Reynolds number ranges 3250–3283 and 3362–3454. Peak energies $\max(E_5)$ and $\max(E_6)$ for the M_5 and M_6 branches are presented as well, which also serves to demonstrate the close relationship between the V_5 and M_5 states for the Reynolds number ranges where they overlap. The Re-ranges of branch extents from experiment [8] are also indicated in figure 7; the agreement in extents is good, and the overlap which brings about a hysteresis in transitions between V and M states is also present in the experimental results.

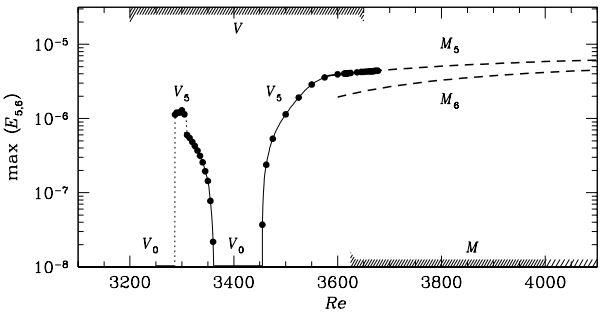

Figure 7: Peak value of energy in leading non-axisymmetric mode, max(E_5), on the V_5 branch, with corresponding values for the M_5 and M_6 branches indicated by dashed lines. The experimental observations of branch extents from [8] are also shown, hatched.

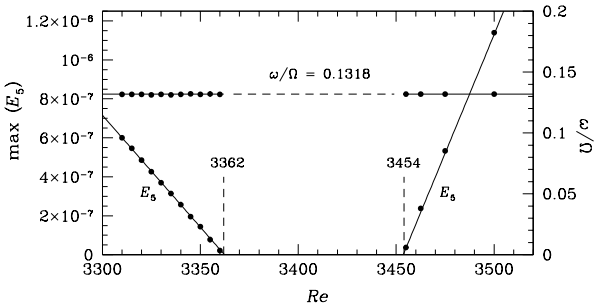

Figure 8: Peak energy in the leading non-axisymmetric mode, E_5, and MRW precession speed, ω/Ω, for the supercritical symmetry-breaking Hopf-type bifurcations on the V solution branch.

The symmetry-breaking behaviour on the V branch at the two bifurcations near $Re = 3362$ and 3454 is examined more closely in figure 8. In both cases max(E_5) rises linearly with changes in Reynolds number. The linear relationships indicate that the amplitude of the MRW varies with $|Re - Re_c|^{1/2}$, identifying these bifurcations from the quasiperiodic axisymmetric V_0 state as being of supercritical Hopf type. Figure 8 also shows that the MRW precession speed $\omega/\Omega = 0.1318$ for both bifurcations. To three significant figures this is the same value as found on the M_6 branch at $Re = 4000$. Arguments presented by Knobloch [5] demonstrate that, near the bifurcation, RW speeds have the form $\omega/\Omega = C_1 - C_2|Re - Re_c|$; here $C_2 \approx 0$ and $C_1 = 0.1318$ for both V_5 states, presumably owing to a high degree of similarity between between the V_0 states from which each V_5 MRW bifurcates at $Re = 3362$ and 3454.

Discussion and Conclusions

Our investigations have shown that for $\Lambda = 2.5$, the initial Re-bifurcation from the axisymmetric, steady, "basic state" is to a periodic flow that retains axisymmetry, following which another set of bifurcations occur that produce solutions which are unstable to symmetry-breaking rotating waves. Comparison with the linear stability analysis of the basic state [6] shows that the A branch is associated with the first eigenmode to lose stability ($Re = 2707$) and that the M branch is associated with the third (which bifurcates at $Re = 3150$). However the V branch would appear to be mixed-mode behaviour which involves both the second bifurcating mode ($Re = 3050$) and the third—definitely it has a contribution from the third mode, as is demonstrated by the nature of the eventual transition of the V branch to the M branch at the upper Re-limits.

Most previous work on flows with RW symmetry-breaking has concentrated on the Taylor–Couette system, where the first unsteady behaviour with increasing Reynolds numbers manifests as rotating waves, however these correspond to another steady flow when observed in an appropriate rotating reference frame. Subsequently either wave modulations or VLF behaviour can appear [10] as a precursor to chaos. Here we have a new scenario, in which axisymmetric modulations appear first, followed by rotating waves that are modulated directly by the underlying axisymmetric flow. In addition we have observed period-doubling-on-torus behaviour that leads not to chaos but back to an axisymmetric state.

Acknowledgement

We gratefully acknowledge support of APAC and its staff.

References

[1] Blackburn, H. M. and Lopez, J. M., Symmetry Breaking of the Flow in a Cylinder Driven by a Rotating Endwall, *Phys. Fluids*, **12**, 2000, 2698–2701.

[2] Blackburn, H. M. and Lopez, J. M., Modulated Rotating Waves in an Enclosed Swirling Flow, *J. Fluid Mech.*, 2001, Submitted.

[3] Escudier, M. P., Observations of the Flow Produced in a Cylindrical Container by a Rotating Endwall, *Exp. Fluids*, **2**, 1984, 189–196.

[4] Gelfgat, A. Y., Bar-Yoeseph, P. Z. and Solan, A., Three-Dimensional Instability of Axisymmetric Flow in a Rotating Lid–Cylinder Enclosure, *J. Fluid Mech.*, **438**, 2001, 363–377.

[5] Knobloch, E., Bifurcations in Rotating Systems, in *Lectures in Solar and Planetary Dynamos*, editors M. R. E. Proctor and A. D. Gilbert, Cambridge University Press, 1994, 331–372.

[6] Lopez, J. M., Marques, F. and Sanchez, J., Oscillatory modes in an enclosed swirling flow, *J. Fluid Mech.*, **349**, 2001, 109–129.

[7] Marques, F., Lopez, J. M. and Shen, J., Mode Interactions in an Enlcosed Swirling Flow: A Double Hopf Bifurcation Between Azimuthal Wavenumbers 0 and 2, *J. Fluid Mech.*, 2001, Accepted.

[8] Stevens, J. L., Lopez, J. M. and Cantwell, R. J., Oscillatory Flow States in an Enclosed Cylinder with a Rotating Endwall, *J. Fluid Mech.*, **389**, 1999, 101–118.

[9] Vogel, H. U., Experimentelle Ergebnisse über die laminare Strömung in einem zylindrischen Gehäuse mit darin rotierender Scheibe, Tech. Rep. 6, Max-Planck-Inst., 1968.

[10] von Stamm, J., Gerdts, U., Buzug, T. and Pfister, G., Symmetry Breaking and Period Doubling on a Torus in the VLF Regime in Taylor–Couette Flow, *Phys. Rev. E*, **54**, 1996, 4938–4957.